Materials Science and Engineering C 50 (2015) 300–308

Contents lists available at ScienceDirect

Materials Science and Engineering C

journal homepage: www.elsevier.com/locate/msec

Ocular biocompatibility evaluation of hydroxyl-functionalized graphene

Mimi Lin [a,1], Ruitao Zou [a,1], Haiyan Shi [a], Shanshan Yu [a], Xiaojian Li [a], Rui Guo [a], Lu Yan [a], Guoxing Li [a], Yong Liu [a,*], Liming Dai [a,b,**]

[a] Institute of Advanced Materials for Nano-Bio Applications, School of Ophthalmology & Optometry, Eye Hospital, Wenzhou Medical University, 270 Xueyuan Xi Road, Wenzhou, Zhejiang 325027, China

[b] Center of Advanced Science and Engineering for Carbon (Case4Carbon), Department of Macromolecular Science and Engineering, Case Western Reserve University, Cleveland, OH 44106, United States

ARTICLE INFO

Article history:
Received 10 September 2014
Received in revised form 27 December 2014
Accepted 30 January 2015
Available online 31 January 2015

Keywords:
Hydroxyl-functionalized graphene (G-OH)
Caspase-3
Western blot
Flow cytometry
Comet assay
Reactive oxygen species (ROS)
Intraocular pressure (IOP)
Electroretinography (ERG)

ABSTRACT

We have presented our recent efforts on genotoxicity and intraocular biocompatibility of hydroxylated graphene (G-OH) prepared by ball milling. We have previously demonstrated that the as-synthesized G-OH could be considered as an excellent alternative for graphene oxide which had been applied widely. Following our last report on G-OH, we carried out detailed studies on genotoxicity and in vivo biocompatibility of G-OH in this work. Less than 5% enhanced caspase-3 level was observed for cells exposed to more than 50 μg/mL G-OH over 72 h, suggesting G-OH caused cell apoptosis was slight. The G-OH induced DNA damage was also found to be mild since expression of p53 and ROS regeneration level was quite low even at high concentration of G-OH over a long time. Cell viability was found to be higher than 90% with 50 μg/mL G-OH and 80% with 100 μg/mL G-OH using flow cytometry. Comet results suggested that less than 5% tail could be found with 100 μg/mL G-OH. TEM results confirmed that G-OH could penetrate into and out of the cytoplasm by means of endocytosis and exocytosis without causing damage on cell membranes. In vivo biocompatibility of G-OH was studied by intravitreal injection of G-OH into rabbits. The ocular fundus photography results showed that G-OH could be diffused in the vitreous body gradually without any damage caused. Injection of G-OH had caused few damages on eyesight related functions such as intraocular pressure, electroretinogram and histological structures of the retina.

1. Introduction

Graphene and its derivatives have attracted intensive attention since its discovery in 2004 [1] due to their unique excellent physical and chemical properties [1–5]. Particularly, graphene oxide (GO), due to its high solubility in water and many other common polar solvents, and rich oxygen-containing functional groups which are ready for device assembly, has been considered as the most exciting graphene based candidate for biological and biomedical applications [6–10]. It is necessary to evaluate biocompatibility of graphene and its derivatives both in vitro and in vivo for their potential applications.

Furthermore, chemical functional groups modified on graphene have showed much influence on its interaction with biomolecules. For instance, Lee et al. have demonstrated promising applications of graphene and graphene oxide to be biocompatible, transferable, and implantable platforms for stem cell growth and differentiation [11]. Insulin was found to be denatured on graphene via strong π–π interaction while no insulin denaturation was observed on graphene oxide (due to the presence of H-bond and electrostatic interaction which facilitated its binding capacity for insulin and enhanced adipogenic differentiation). Another type of graphene derivative, graphene nanogrids prepared from oxidative unzipping of multi-walled carbon nanotubes were found to be excellent capacity in the adsorption of the chemical inducers which accelerated differentiation of human mesenchymal stem cells [12]. In another study, Akhaven and co-worker found out that UV-assisted photocatalytically reduced GO/TiO_2 hybrid accelerated differentiation of human neural stem cells into neurons, associating with electron injection from the photoexcited TiO2 into the cells on the reduced GO via Ti–C and Ti–O–C bonds [13].

Numerous scientists have reported the cytotoxicity of both graphene and GO [14–22], more recent studies are focused on genotoxicity of graphene based materials particularly the effects of chemical modification of graphene on genotoxicity. For example, Akhavan's group measured various genotoxicities of GO, hydrazine reduced GO (N_2H_4-rGO), hydrothermally reduced GO (HT-rGO), and green tea polyphenols reduced GO (GTP-rGO) with spermatozoa [23]. The highest genotoxicity was observed at the N_2H_4-rGO due to its ultra sharp edge and high mobility which facilitated the penetration of nanomaterials into spermatozoa and interaction with the cell nuclei, while the lowest genotoxicity

* Corresponding author.
** Correspondence to: L. Dai, Institute of Advanced Materials for Nano-Bio Applications, School of Ophthalmology & Optometry, Eye Hospital, Wenzhou Medical University, 270 Xueyuan Xi Road,Wenzhou, Zhejiang 325027, China.
E-mail addresses: yongliu1980@hotmail.com (Y. Liu), liming.dai@case.edu (L. Dai).
[1] These authors contribute equally.

http://dx.doi.org/10.1016/j.msec.2015.01.086
0928-4931/

was observed at GTP-rGO since steric effect was induced by the GTP attached on the rGO. Size- and concentration-dependent cytotoxicity and genotoxicity of reduced graphene oxide nanoplatelets with human mesenchymal stem cells were also reported [24]. Reduced graphene oxide nanoribbons (prepared from oxidative unzipping of multi-walled carbon nanotubes) were found to penetrate into the human mesenchymal stem cells and cause DNA fragmentation and chromosomal aberrations even at low concentration (e.g. 1.0 μg/mL within 1 h) while much lower genotoxicity was observed at the reduced graphene nanosheets, suggesting that different inner structures of graphene derivatives played an essential role in their interaction with cells and corresponding biocompatibility [25].

In our previous work, we have demonstrated the preparation of the large-scaled graphene via a novel modified ball milling technique [26,27]. The as-prepared hydroxylated graphene (G-OH) exhibited much better properties than GO in many aspects including electroactivity and biocompatibility with human retinal pigment epithelium (RPE) cells (the cell viability with G-OH was higher than 80% after 4 days' culturing [27] compared to the 60% cell viability with GO after 3 days' culturing [28]), while remaining many advantages of GO such as water solubility and processability [27]. Moreover, the reported ball milling technique is a simple but efficient, environmentally-friendly graphene preparation method without the use of any toxic chemicals. G-OH is thus considered as an excellent candidate for various application areas where GO is utilized. Though we have carried out some preliminary cytotoxicity studies (such as CCK-8 for cell viability, LDH for cell membrane integrity, and fluorescent micrography for cell apoptosis) on G-OH in our previous work [27], it is necessary to perform further biocompatibility studies such as genotoxicity and in vivo evaluation on G-OH for applications especially in biology and biomedicine. Due to unique properties and toxicity mechanism of nanomaterials particularly carbon nanomaterials [29,30], genotoxicity studies on G-OH is essential for its further large-scaled applications and commercialization. Particularly eye contact is inevitable for many areas involving G-OH e.g. research, industry production, transportation and other related areas. Detailed in vivo ocular biocompatibility evaluation on G-OH is thus necessary. In this work, we have carried out detailed genotoxicity evaluation on G-OH including caspase 3 activity, western blots, flow cytometry, comet assay, ROS generation, and transmission electronic microscopy. Furthermore, the influence of G-OH on eyesight related functions such as intraocular pressure, electroretinogram and histological structures of retina has been discussed.

2. Materials and methods

2.1. Materials and reagents

Graphite flakes were obtained from Qingdao Haida Corporation. 12 Zelanian white rabbits as experimental animals were provided by Experimental Animal Center of Wenzhou Medical University. TobraDex eye ointment and Proxymetacaine eye drops were from Alcon Corporation. Balance salty solution (BSS) was purchased from Alcon Corporation. All other chemicals were obtained from Sigma-Aldrich.

2.2. Preparation of hydroxyl-graphene (G-OH)

G-OH was prepared by the ball milling technique as we reported elsewhere [27]. Briefly, graphite and potassium hydroxide were mixed at the mass ratio of 1:10–1:30 and vigorously shaken at the speed of 200–400 rpm for 8–12 h by ball milling. The resulting material was then removed by deionized (DI) water and further centrifuged at 2000 rpm for 20 min. The residual impurities were removed using a dialysis bag prior to biocompatibility measurements on the final products.

2.3. G-OH induced ARPE-19 cell apoptosis analysis

ARPE-19 cell is a cell line derived from human RPE. ARPE-19 cells seeded in 6-well plates at a density of 3×10^5 cells/well were incubated with G-OH at different concentrations of 5, 10, 50 and 100 μg/mL for 24, 48 and 72 h respectively. Cells were harvested and lysed in protein buffer. BCA (bicinchoninic acid) method was used to calculate the extracted protein concentrations. The protein samples were detected with expression of caspase-3 and p53 respectively.

2.4. Flow cytometry analysis

ARPE-19 cells were incubated with G-OH at different concentrations of 5, 10, 50 and 100 μg/mL for 24, 48 and 72 h and were subsequently collected into centrifuge tubes, respectively. The cells incubated with 0.5 M H_2O_2 for 20 min at 4 °C were used as the positive control while the cells incubated without the addition of nanomaterials were employed as the negative control. The cells were washed twice using cold phosphate buffer solution (PBS pH 7.4) and re-suspended in binding buffer at a density of 106/mL. 100 μL cell suspension was transferred to a 1.5 mL EP tube, with the addition of 5 μL Fluorescein Isothiocyanate (FITC) Annexin and 5 μL Propidium Iodide (PI). The cells were vortexed gently and incubated for 15 min at room temperature in the dark. 400 μL of binding buffer was then added to each tube prior to be analyzed using flow cytometry.

2.5. Comet assay

ARPE-19 cells were incubated with G-OH at different concentrations ranging from 5 to 100 μg/mL over 24, 48 and 72 h, respectively. The cells incubated with 0.5 M H_2O_2 for 10 min at 37 °C were used as the positive control while cells without addition of nanomaterials were used as the negative control. After being washed twice by cold PBS, the cells were resuspended by cold PBS at a density of 10^{5-6}/mL. 1 mL solution of 1% NMA (Normal Melting-point Agarose) dissolved in double-distilled water (ddH_2O) was spread on the glass side and then stored at 4 °C for 30 min. 5 μL 1% LMA (Low Melting-point Agarose) mixed with 25 μL cell suspension was dropped onto the first layer of the NMA gel and remained at 4 °C for 30 min. Coverslips were subsequently removed carefully and the slide with the gel was soaked in cell lysis buffer at 4 °C for 2 h. After being washed gently by ddH_2O twice, the slide was soaked in electrophoresis buffer (pH = 13) for 40 min, followed by electrophoresis at 25 V for 25 min. After being washed by ddH_2O twice and PBS once more, the resulting gel was dehydrated by ethanol overnight and dyed with PI at concentration of 30 μg/mL for 15 min in the dark. Images were taken using a fluorescent microscope at 550 nm. 50–100 comets were measured for each sample to obtain the percentage of tail DNA in cells.

2.6. Reactive oxygen species (ROS) generation

Possible DNA damage with G-OH was measured using ROS generation level. ARPE-19 cells were cultured in 6-well plate at the density of 10^4 cells/well and allowed to adhere to the well bottom for 24 h. The G-OH with concentrations varied from 5 μg/mL to 100 μg/mL was introduced into the culture media and co-cultured with cells over 24 h, 48 h, and 72 h, respectively. A 10 μM DCFH-DA was then introduced into the culture media and incubated for 20 min. The resulting media was subsequently removed and the well was rinsed using PBS three times to remove extra DCFH-DA, followed by the addition of a fresh culture media. Fluorescence intensity was determined using SpectraMas M5 Microplate reader on 488 nm excitation wavelength and 525 emission wavelength.

2.7. Transmission electronic microscopy (TEM)

ARPE-19 cells were fixed using 2.5% glutaraldehyde solution at 4 °C overnight. The cells were subsequently washed by PBS (pH 7.4) prior to be fixed by 1% osmic acid for 1 h. The collected cells were then washed using deionized water twice and dipped in 1% uranyl acetate solution at 37 °C for 1 h. The cells were then transferred into various acetone solutions for gradient dehydration and embedding-liquid at 37 °C overnight. Subsequently the cells were soaked in embedding-liquid at 45 °C for 1 h, followed by embedding with polymerizing liquid till they changed to be solid. The cells' super fine slices were consequently obtained and dyed with toluidine blue for TEM characterization.

2.8. Intravitreous injection of G-OH

200 μg, 122.47 μg and 75 μg G-OH pre-sterilized at high temperature were dispersed in 50 μL BSS respectively. 12 Zelanian white rabbits were averagely divided into 3 groups with similar weight and sex ratio. Rabbits were anesthetized using an intramuscular injection of 0.2 mL/kg SMX and 3 wt.% pentobarbital sodium (1 mL/kg). Pupils were dilated with mydrin (containing 5 mg/mL tropicamide and 5 mg/mL phenylephrine hydrochloride) and surface anesthetized with proparacaine hydrochloride. 50 μL G-OH suspensions with various concentrations were intravitreally injected into the right eye of the rabbit using a 30-gauge needle inserted 2 mm posterior to the limbus. The same amount of BSS was injected into the left eye used as the control. Levofloxacin eye gel was used on both eyes for three days after operation for prevention from infection.

2.9. Intraocular pressure and ocular examination

The injected eyes were surface anesthetized with proparacaine hydrochloride prior to be measured using Tono-Pen Tonometer (Medtronic Solan Corporation) for IOP. IOP results were repeated more than 5 times to get accurate data. Fundus pictures were taken using a Nikon 505 Fundus Camera (Nikon Corporation) after the rabbit's pupil was dilated with mydrin.

2.10. Electroretinography (ERG)

After dark adaptation for 1 h, the rabbits were anesthetized with an intramuscular injection of 0.2 mL/kg SMX and 3 wt.% 1 mL/kg pentobarbital sodium. Pupils were dilated with mydrin. All steps were operated under the dim red light to remain the dark adaptation state of the rabbits' eyes. A Burian-Allen bipolar ERG contact lens electrode was applied on the surface anesthetized cornea while the two reference electrodes were placed in the skin of eyelids and the ground electrode was placed in the skin of the middle forehead. ERG responses were obtained using a wide band filter (Roland Corporation), stimulating with single full field flashes with −20 dB attenuated white light flash interval 2 ms and standard flash (SF) per 10 ms. Cone responses (SF, 0.5 s) were obtained after light adaptation for 20 min.

2.11. Histologic examination

Rabbits were killed by overdoses of intracardiac ketamine and xylazine 8 weeks after injection and the eyes were collected integrally. The eyes were subsequently fixed in 4% paraformaldehyde, dehydrated with various concentrations of ethanol solutions and embedded in paraffin. 5 μm thick sections were deparaffinized by immersing in xylene and then rehydrated. The resulting materials were then stained with hematoxylin–eosin (H&E) prior to examination using optical microscopy [31].

2.12. Statistical analysis

Statistical analysis was executed using SPSS 18.0. All the experimental data were reported as the mean ± SD. Values were compared by multi-sample comparison tests after performing ANOVA. The significance level was set at $p < 0.05$.

3. Results and discussion

3.1. Dispersibility and morphology

Biotoxicity of nanomaterials has been found to be related to the solubility/dispersibility of nanomaterials in solution [32]. Though various pulmonary toxicities have been reported for GO [33], the biocompatibility of GO can be significantly improved by the incorporation of PEG with GO [34]. The enhanced biocompatibility of GO after the introduction of PEG has been attributed to the improved dispersibility of nanomaterials. We have previously reported that better dispersibility and cytotoxicity of G-OH could be obtained when compared with GO [27]. In this work, further information on cell apoptosis and genotoxicity of G-OH was discussed.

AFM micrograph of the as-synthesized G-OH was shown in Fig. 1. The homogenously dispersed G-OH nanosheets were found dominant, suggesting good exfoliation of graphite via edge-functionalized ball milling process. The single layered G-OH sheet with thickness of around 1.3 nm was observed in Fig. 1, suggesting that a single-layered graphene nanosheet could be obtained. Various characterization techniques including UV–vis spectroscopy, Fourier transform infrared (FTIR), nuclear magnetic resonance analysis (NMR), and Raman and X-ray photoelectron spectroscopy (XPS) have been used to confirm the formation of hydroxyl groups and physicochemical property of G-OH as demonstrated in our previous work [27].

3.2. Caspase 3 activity and western blots

Apoptotic studies on RPE cells with G-OH were determined by caspase 3 activity assay as the activation cytosolic caspase-3, indicating the cell apoptosis [35,36]. As shown in Fig. 2(a), the Caspase-3 activity of ARPE-19 cells cultured with less than 50 μg/mL G-OH over 48 h didn't show much difference. The increased Caspase-3 activity (though less than 5%), however, could be found when more than 50 μg/mL G-OH was introduced over 72 h. Genotoxicity of G-OH with ARPE-19 cells was further investigated by expression of p53 using western blot

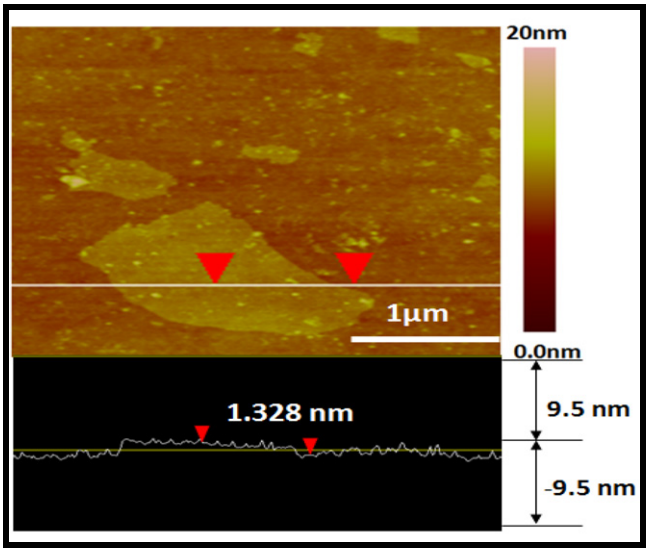

Fig. 1. AFM image of the as-synthesized G-OH.

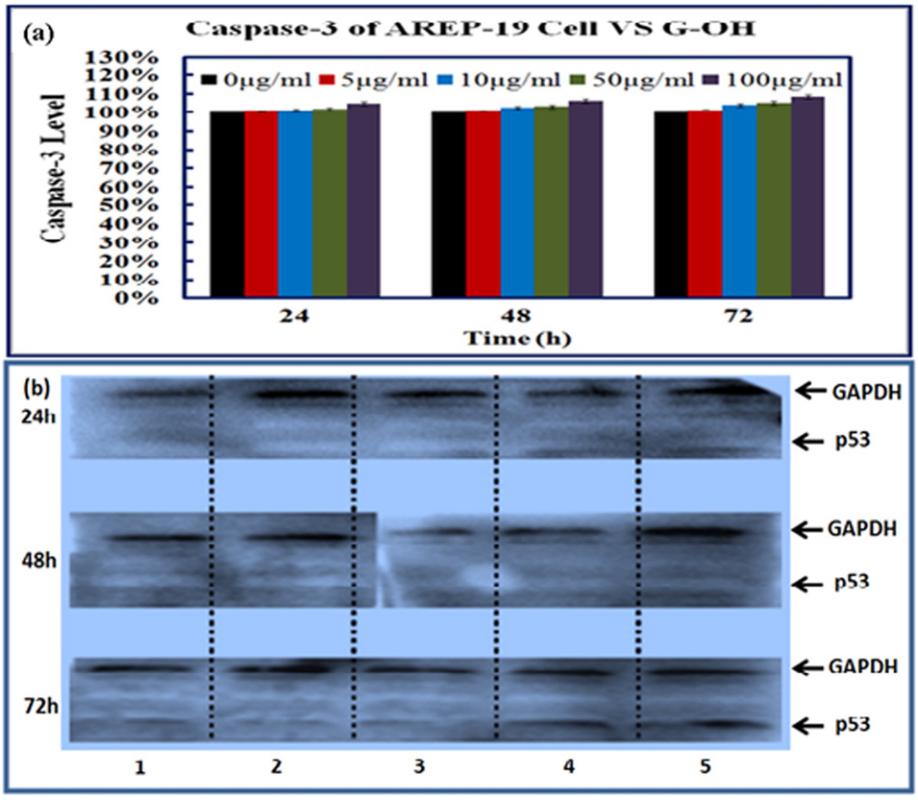

Fig. 2. (a) Expression of caspase-3 after exposure of ARPE-19 cells to various amounts of G-OH over different times, (b) expression of p53 after exposure of ARPE-19 cells over different times to G-OH at various concentrations: 1: the control, 2: 5 μg/mL, 3: 10 μg/mL, 4: 50 μg/mL, and 5: 100 μg/mL.

analysis. p53 is a kind of protein for DNA repairing which generally activated by protein phosphorylation when DNA was damaged [37,38]. Expression of p53 is able to arrest DNA replication and provides time for the DNA damage to be repaired or triggers cell apoptosis if the DNA repair is not successful [30]. As shown in Fig. 2(b), no significant expression of p53 was observed within 48 h, suggesting that no DNA damage was caused within 48 h even though 100 μg/mL G-OH was applied. Expression of p53 could be found (though not significant) when cells were cultured over 72 h with more than 50 μg/mL G-OH introduced. The p53 expression results were well consistent with the Capaspase-3 studies. These results suggest that low content of G-OH (less than 50 μg/mL) will not cause DNA damage even for a long exposure time but a high amount of G-OH (higher than 100 μg/mL) exposed for a long time (over 72 h) may cause some DNA damage and cell apoptosis.

3.3. Flow cytometry

We further carried out flow cytometry on the G-OH induced ARPE-19 cells. The cells cultured without the addition of nanomaterials were used as the negative control (−) while the cells incubated with 0.5 M H_2O_2 for 20 min at 4 °C were used as the positive control (+). As shown in Fig. 3, there are four quadrants in one table. The up-left part shows PI(+)/FITC(−), and the up-right indicates PI(+)/FITC(+) while the down-left part represents PI(−)/FITC(−), and the down-right is PI(−)/FITC(+). FITC(+) suggested that the cells were undergoing apoptosis while PI(−) indicated that the cells were at the end stage of apoptosis or already dead. It was found from Fig. 3(b–e) that only small amounts of the apoptotic cells were observed with the addition of G-OH. The cell viabilities were found to be 97.25% (with 5 μg/mL G-OH), 96.43% (with 10 μg/mL G-OH), 90.7% (with 50 μg/mL G-OH) and 80.82% (with 100 μg/mL G-OH) respectively, compared to the 80.25% for the cells incubated without nanomaterials (Fig. 3(a)). The results confirmed that G-OH did no harm to the RPE cells, well consistent with the results from caspase 3 activity and western blots. Cytotoxicity of G-OH was found to be much lower than that of GO (generally 60% cell viability [28]).

3.4. Comet test

To further identify genotoxicity of the GOH with ARPE-19 cells, we carried out the Comet test. As shown in Fig. 4(a), there was no obvious tails observed in the fluorescent images when ARPE-19 cells were incubated with G-OH varied from 5 μg/mL to 50 μg/mL over 24 h. But there was small amout of tails found (less than 5%) when the G-OH concentration was 100 μg/mL. Similar results were obtained when the culture time was increased to 48 h and 72 h (Figure S1(a) and (b)). The percentages of tail DNA detected during Comet test were recorded and calculated. The results further confirmed that no significant differences between the negative control and cells incubated with nanomaterials (Fig. 4(b)). Some tails observed at the sample with 100 μg/mL G-OH were ignorable when compared with the positive control. The Comet results suggested that the G-OH showed little genotoxicity with ARPE-19 cells at small dose while a bit genotoxicity was found when the concentration of G-OH was higher than 100 μg/mL. No time-dependent toxicity was observed.

3.5. ROS generation

ROS generation level is associated with oxidative stress level in cells. As shown in Fig. 5, ROS generation in ARPE-19 cells increased with increasing amounts of G-OH. When the concentration of G-OH was less than 10 μg/mL, the changes in ROS level were less than 10%. But ROS generation became more significant when the content of G-OH was more than 50 μg/mL. A 18% ROS generation increase was obtained at the sample with 100 μg/mL G-OH. The ROS generation showed dose-

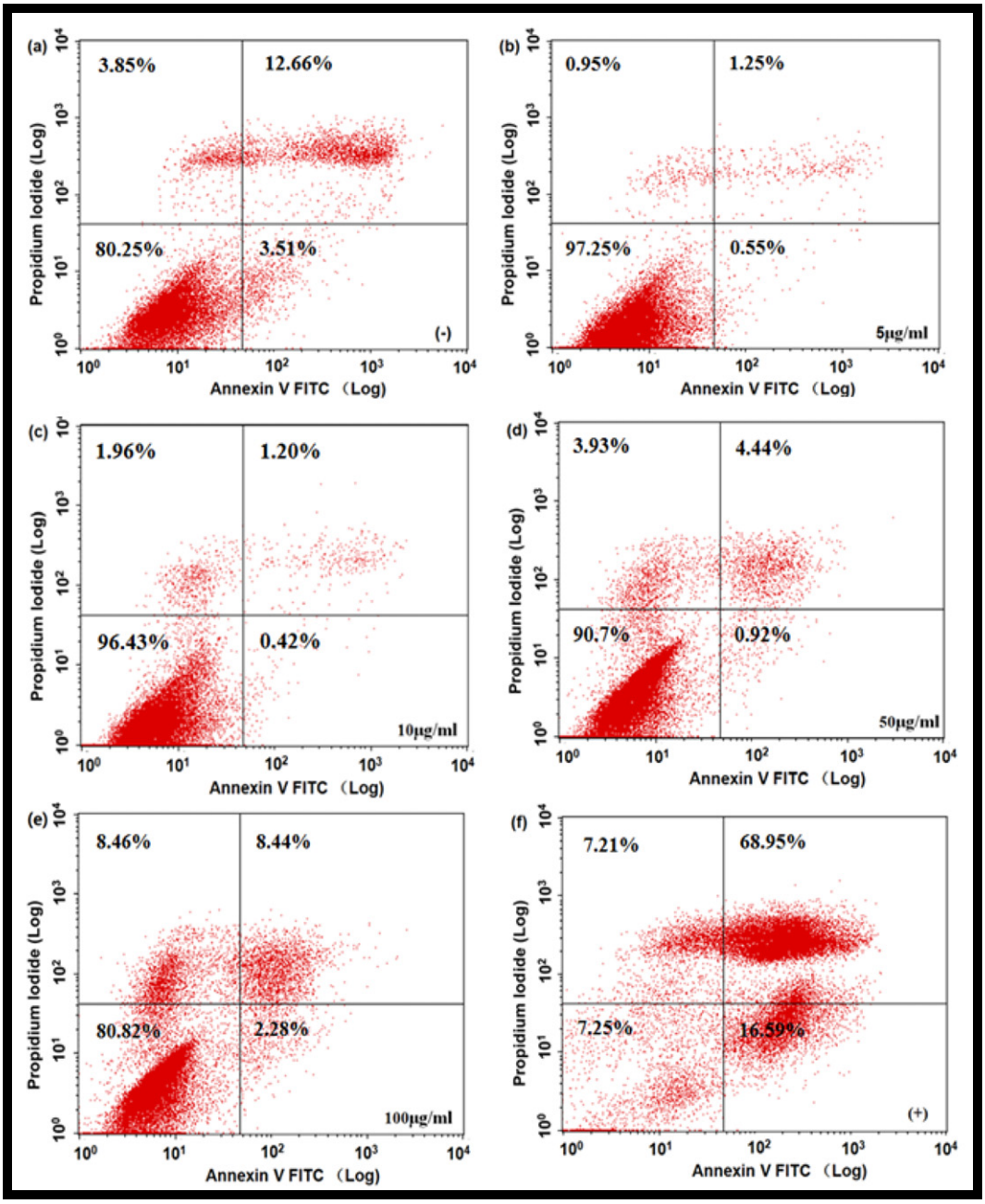

Fig. 3. Flow cytometry analysis of ARPE-19 cells incubated with G-OH at different concentrations: (a) the negative control (nothing special added), (b) 5 μg/mL, (c) 10 μg/mL, (d) 50 μg/mL, (e) 100 μg/mL, and (f) the positive control (0.5 M H_2O_2).

dependent changes while no time-dependent trends were observed, suggesting that higher amounts of GOH (more than 100 μg/mL) might cause some DNA damage via oxidative stress.

3.6. TEM results

Fig. 6 showed TEM images of ARPE-19 cells exposed to G-OH after various times. The presence of G-OH around the cell was abundant while small amounts of G-OH were found inside the karyotheca when cells were exposed over 24 h. But no visible damage or change on cell morphology was observed while liquor bubble was increased and expanded a bit. Increased amounts of phagocytosis bubbles with G-OH and G-OH inside karyotheca were significant when cells were exposed over 48 h. When the incubation time was increased to 72 h, however, no G-OH inside the cell was visible any more. G-OH was found to be released from the cell while nucleus and organelles remained intact. This interesting finding, along with our previous LDH studies on G-OH induced ARPE cells [27], suggested that penetration of G-OH into and out of the cytoplasm by means of endocytosis and exocytosis did not damage cell membranes as "other nanomaterials" [39,40].

3.7. Intraocular pressure (IOP)

We further carried out intraocular biocompatibility of G-OH in vivo by intravitreal injection of G-OH into Zelanian white rabbits. For the purpose of analysis, a relative IOP value ($R_{IOP} = IOP_{injected} / IOP_{control}$) was utilized. As shown in Figs. 7(a) and 5(b), the values of R_{IOP} fluctuated in the range of 100% ± 20%, which could be considered as the normal IOP fluctuation range as reported elsewhere [41–43]. The injection of G-OH thus caused limited influence on the rabbit's IOP.

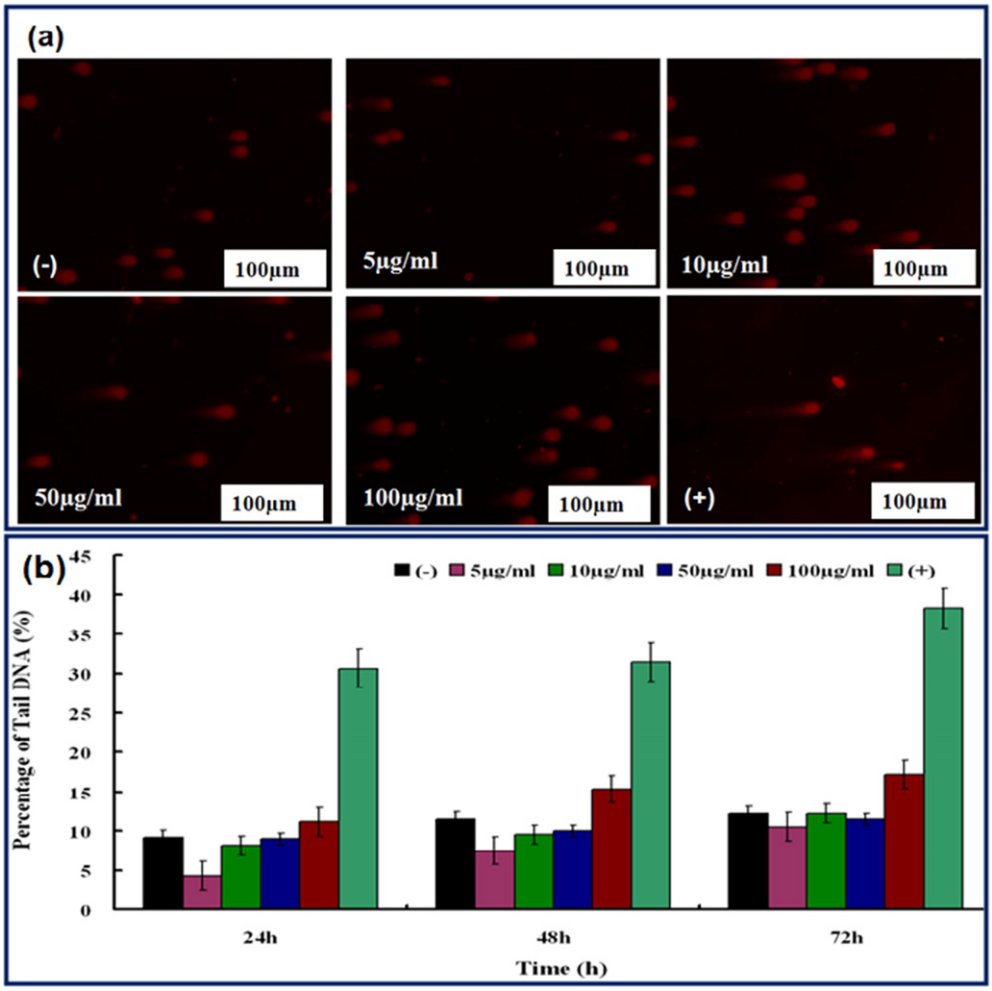

Fig. 4. (a) The fluorescent images of ARPE-19 cells incubated with G-OH at different concentrations for 24 h, and (b) the percentages of tail DNA detected during the COMET test. The negative control is the cells without nanomaterials while the positive control is the cells cultured with 0.5 M H_2O_2.

3.8. Fundus photos

Fig. 8 shows the fundus photos for the rabbits' eyes after injection using slit-lamp biomicroscopy and fundoscopy at the baseline. When G-OH at the high concentration (200 μg/50 μL BSS) was injected into the vitreous body, the injected G-OH was found to be a gel shape with a clear border in vitreum. The gel border became illegible and better dispersion of the injected stuff was observed with decreasing G-OH content injected. The decrease of G-OH in the vitreous body was significant with increasing time. No more residual G-OH was visible after injection for 4 weeks, indicating possible diffusion of G-OH. We also found that the introduction of G-OH didn't cause any damage on most parts of the rabbit eyes such as corneas, anterior media, posterior media, and retinas.

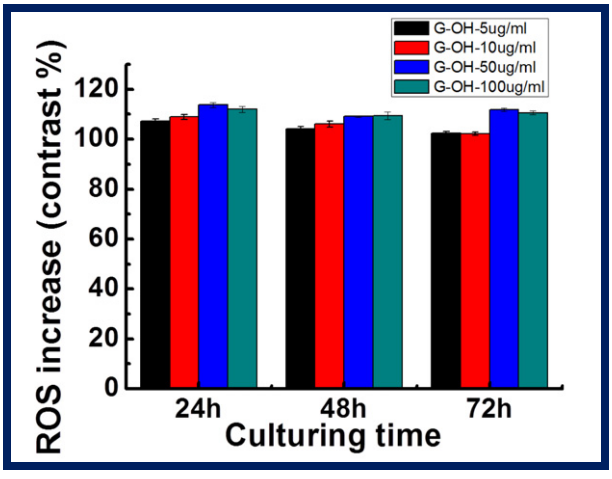

Fig. 5. ROS generation changes after exposure of cells to various concentrations of G-OH over 24 h, 48 h, and 72 h respectively.

3.9. Electroretinography (ERG)

We further carried out ERG measurements on the experimental rabbits to identify the influence of G-OH on the eyesight functions. ERG is a recording of characteristic sequence of electrical potentials generated within the retina when it is stimulated by a flash of light. ERG can be used to detect the loss of eyesight functions related to various cells such as cone cells, rod cells and bipolar cells. As shown in Fig. 9(a) and (b), ERG tracings of the injected eyes both from the dark-adapted and the light-adapted were similar to that of the control eyes. A relative ERG ($R_{ERG} = ERG_{injected} / ERG_{control}$) was used to identify the changes of ERG more visually. Variation of the amplitudes (A Wave and B Wave) in both the dark adaptation (Fig. 9(c)) and the light adapted state (Fig. 9(d)) is less than 20%. Less than 30% ERG amplitude change was generally considered to be indistinctive [41–43]. EGR results suggested that the injection of G-OH didn't cause too much adverse impact on the eyesight functions.

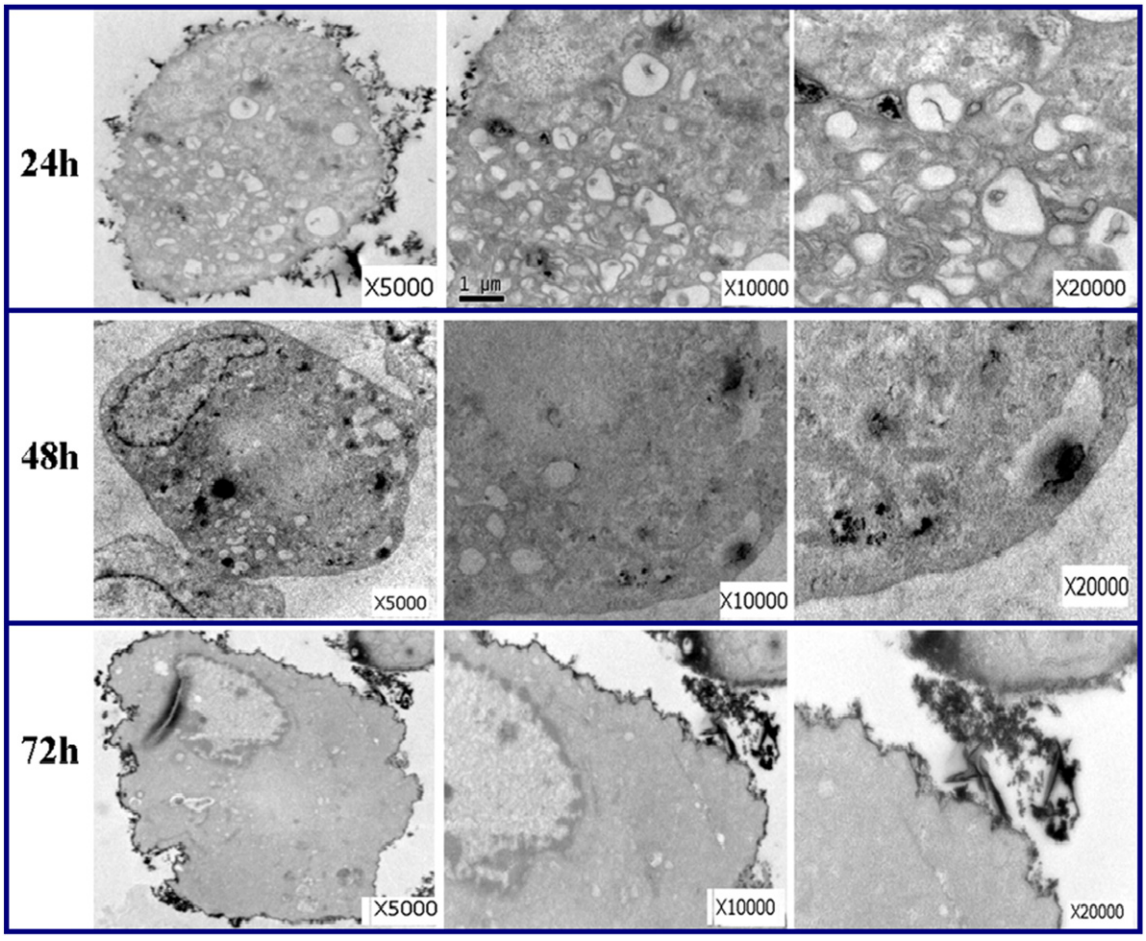

Fig. 6. TEM of ARPE-19 cells incubated with G-OH over different times.

3.10. Histologic examination

After euthanasia of the rabbits, we took the eyeballs completely and fixed them in 4% paraformaldehyde. The eyeballs were subsequently cut through the optic disc along the superior rectus muscle into two halves average. After HE staining, sections were shown in Fig. 10. It could be found that the retina showed clear layered and complete structures, and no abnormal cell morphologies were observed, suggesting that the injected G-OH didn't cause damage of the retina.

4. Conclusions

Our preliminary results demonstrated the ocular genotoxicity and biocompatibility of the novel graphene derivative-G-OH. G-OH

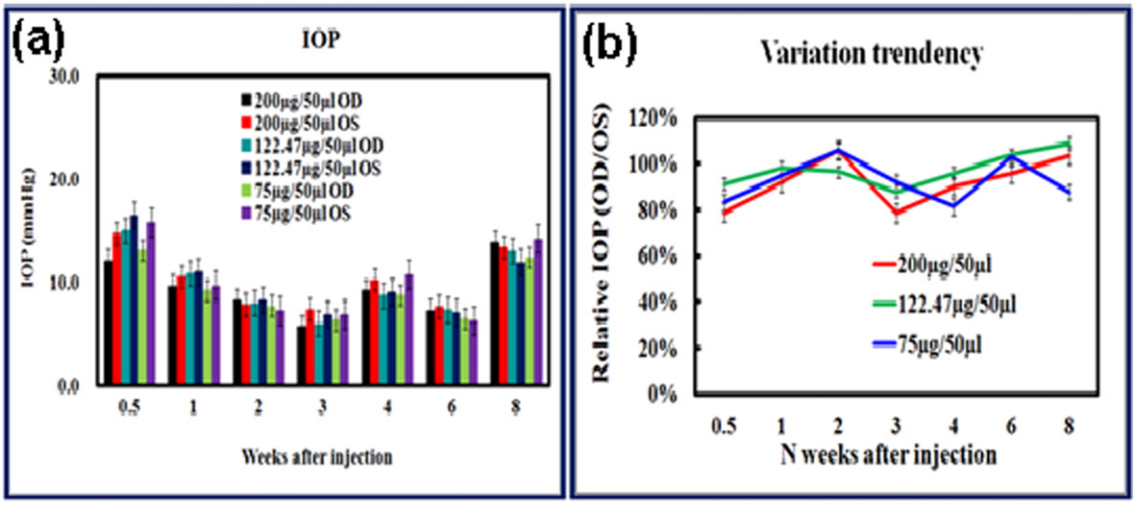

Fig. 7. (a) IOP results from G-OH intravitreally injected rabbits. OD represents the injected eye and SD is the control eye. (b) Relative IOP variation after injection over various weeks.

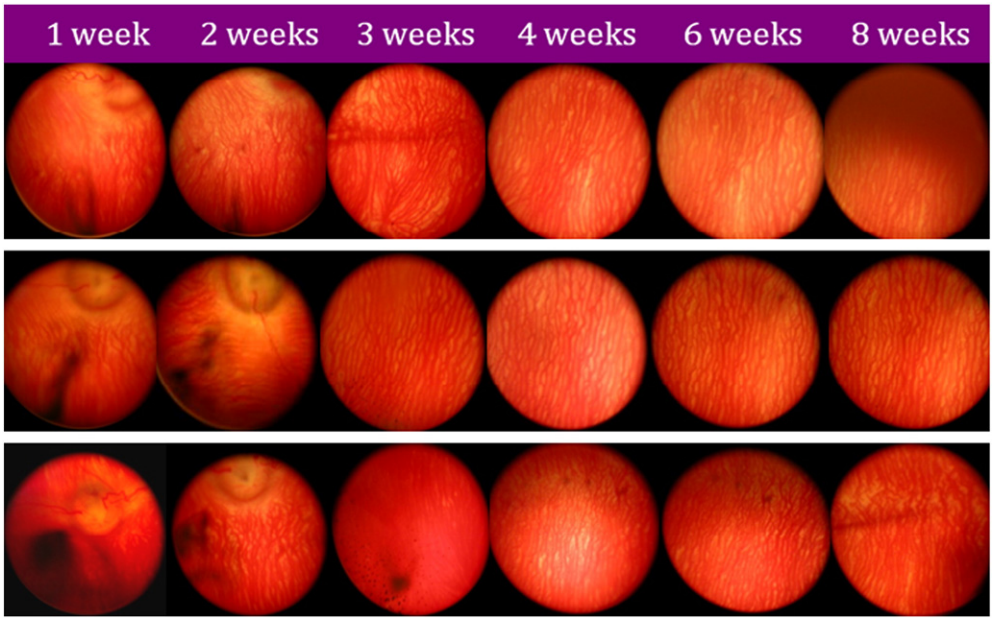

Fig. 8. Slim-lamp fundus photos of intravitreally injected eyes after injection of 75 μg G-OH, 122.47 μg G-OH and 200 μg G-OH in 50 μL BBS over 1 week, 2 weeks, 3 weeks, 4 weeks, 6 weeks, and 8 weeks.

prepared by ball milling was considered as an excellent alternative for GO which were utilized in a great range of application areas. Following our previous work on preparation and preliminary cytotoxicity evaluation of G-OH, we carried out further detailed genotoxicity and in vivo measurements on G-OH in this work. It was found out that general amount of G-OH didn't cause any RPE cell apoptosis and DNA damage within 48 h while a small proportion of cell apoptosis and DNA damage could be found when cells were exposed to higher than 50 μg/μL G-OH over 72 h. Cell viability with less than 50 μg/μL G-OH was found to be more than 90%, a much higher improved biocompatibility compared with the widely used GO. Both expressions of caspase-3 and p53, however, showed dose and time dependent increasing trends. Comet and ROS results also exhibited dose-dependent increasing trends while no time dependent change was observed. Possible genotoxicity induced by G-OH may occur when the concentration of G-OH is higher than 100 μg/mL. Our results suggest that suitable eye protection was necessary for people dealing with graphene-based materials frequently. Intravitreous injection of G-OH into rabbits (even 200 μg/50μL BSS) gradually decreased after 4 weeks without any damage on cell morphology, structures, and most parts of eyes. We also found that intravitreous

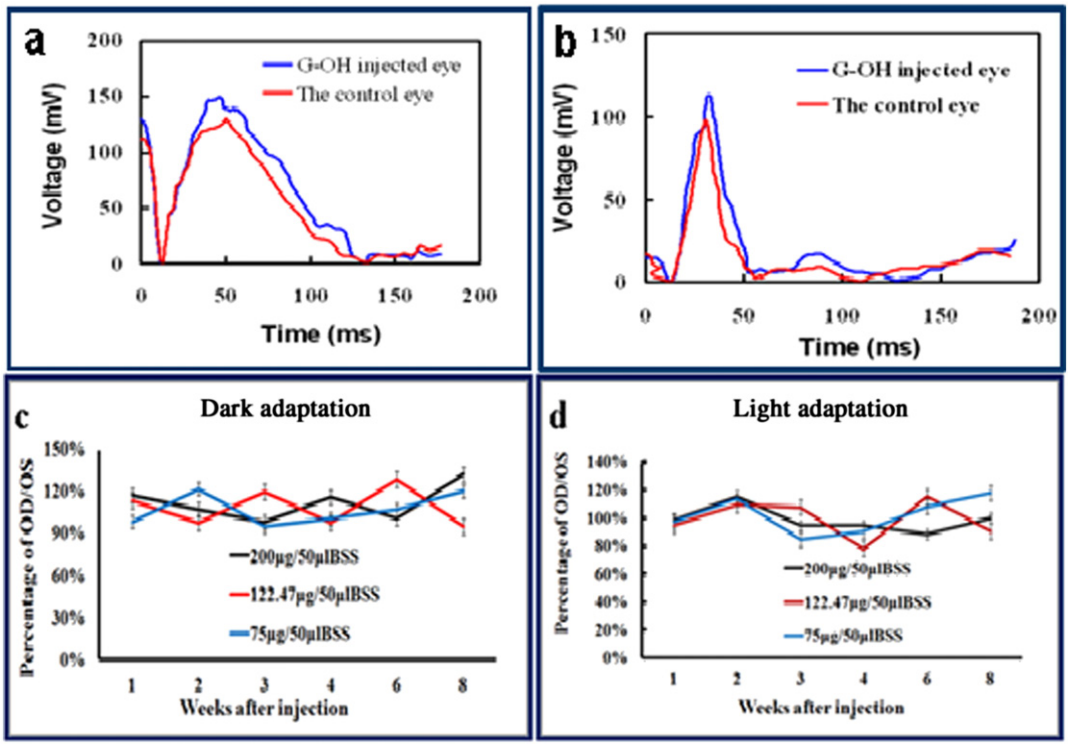

Fig. 9. Electroretinograms of (a) Dark adaptation curve, (b) light adaptation curve, (c) A Wave amplitude relative fluctuation, and (d) B Wave amplitude relative fluctuation at G-OH injected rabbits' eyes.

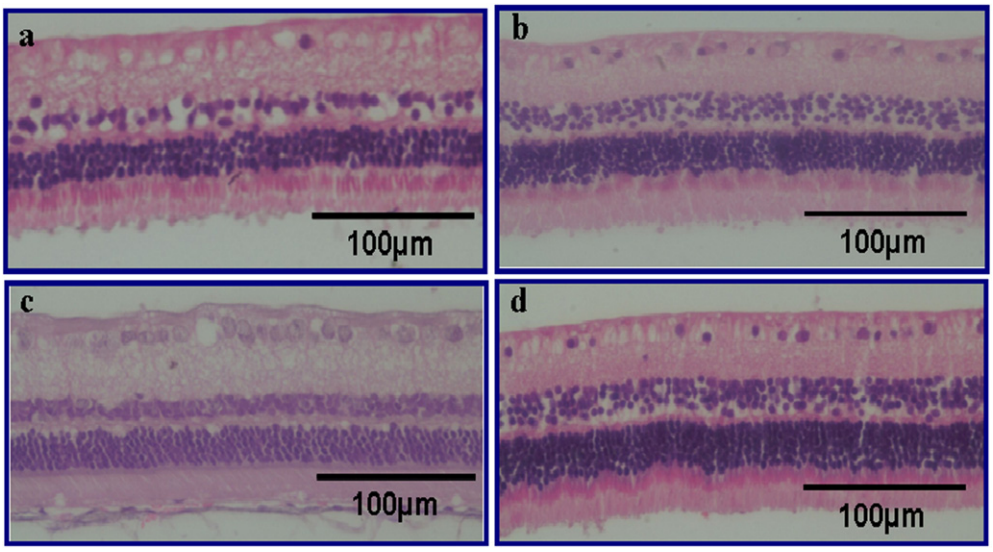

Fig. 10. Histological HE staining sections of (a) the control, (b) 75 μg G-OH, (c) 122.47 μg G-OH, and (d) 200 μg G-OH in 50 μL BBS intravitreally injected rabbits after injection for 8 weeks respectively.

injection of G-OH caused few changes on eyesight related functions such as IOP, ERG and retinal structures. All results in this work suggested that G-OH didn't cause significant adverse effects on ocular systems but genotoxicity of G-OH with RPE cells might present when a large amount of G-OH was utilized for a long time, providing useful safety information for persons who regular dealing with graphene-based materials and other nanomaterials.

4.1. Ethical conduct of research

The authors state that they have obtained approval from the Wenzhou Medical University Animal Care and Use Committee, and have followed the principles outlined in the Declaration of Helsinki for all human or animal experimental investigations. In addition, for investigations involving human subjects, informed consent has been obtained from the participants involved.

Acknowledgements

Authors are grateful to Prof. Ling Hou (Wenzhou Medical University) for kindly providing ARPE-19 cells. Financial supports for this work from the Chinese National Nature Science Foundation (21374081, 81301320, 51433005), the Scientific Research Foundation for the Returned Overseas Chinese Scholars, the Zhejiang National Nature Science Foundation (Y13H180013, LQ14C100002), and the Wenzhou Bureau of Science and Technology (Y20080087) are acknowledged.

Appendix A. Supplementary data

Supplementary data to this article can be found online at http://dx.doi.org/10.1016/j.msec.2015.01.086.

References

[1] K.S. Novoselov, A.K. Geim, S.V. Morozov, D. Jiang, Y. Zhang, S.V. Dubonos, I.V. Grigorieva, A.A. Firsov, Science 306 (2004) 666–669.
[2] A.K. Geim, K.S. Novoselov, Nat. Mater. 6 (2007) 183–191.
[3] Y. Zhang, Y. Tan, H.L. Stormer, P. Kim, Nature 438 (2005) 201–204.
[4] I.W. Frank, D.M. Tanenbaum, A.M. Zande, P.L. McEuen, J. Vac. Sci. Technol. B 25 (2007) 2558–2561.
[5] M. Hirata, T. Gotou, S. Horiuchi, M. Fujiwara, M. Ohba, Carbon 42 (2004) 2929–2937.
[6] Y. Liu, D. Yu, C. Zeng, Z. Miao, L. Dai, Langmuir 26 (2010) 6158–6160.
[7] X. Sun, Z. Liu, K. Welsher, J.T. Robinson, A. Goodwin, S. Zaric, H. Dai, Nano Res. 1 (2008) 203–212.
[8] W. Hu, C. Peng, W. Luo, M. Lv, X. Li, D. Li, Q. Huang, C. Fan, ACS Nano 4 (2010) 4317–4323.
[9] W. Zhang, Z. Guo, D. Huang, Z. Liu, X. Guo, H. Zhong, Biomaterials 32 (2011) 8555–8561.
[10] P. Huang, C. Xu, J. Lin, C. Wang, X. Wang, C. Zhang, X. Zhou, S. Guo, D. Cui, Theranostics 1 (2011) 240–250.
[11] W.C. Lee, C.H. Lim, H. Shi, L.A. Tang, Y. Wang, C.T. Lim, K.P. Loh, ACS Nano 5 (2011) 7334–7341.
[12] O. Akhavan, E. Ghaderi, M. Shahsavar, Carbon 59 (2013) 200–211.
[13] O. Akhavan, E. Ghaderi, Nanoscale 5 (2013) 10316–10326.
[14] W. Kan, R. Jing, S. Hua, J. Zhang, Y. Wo, S. Cuo, D. Cui, Nanoscale Res. Lett. 6 (2011) 1–8.
[15] Y. Zhang, S.F. Ali, E. Dervishi, Y. Xu, Z. Li, D. Casciano, A.S. Biris, ACS Nano 4 (2010) 3181–3186.
[16] S.R. Ryoo, Y.K. Kim, M.H. Kim, D.H. Min, ACS Nano 4 (2010) 6587–6598.
[17] H. Chen, M.B. Müller, K.J. Gilmore, G.G. Wallace, D. Li, Adv. Mater. 20 (2008) 3557–3561.
[18] S. Park, N. Mohanty, J.W. Suk, A. Nagaraja, J. An, R.D. Piner, W. Cai, D.R. Dreyer, V. Berry, R.S. Ruoff, Adv. Mater. 22 (2010) 1736–1740.
[19] K. Liao, Y. Lin, C.W. Macosko, C.L. Haynes, ACS Appl. Mater. Interfaces 3 (2011) 2607–2615.
[20] N.V. Vallabani, S. Mittal, R.K. Shukla, A.K. Pandev, S.R. Dhakate, R. Pasricha, A. Dhawan, J. Biomed. Nanotechnol. 7 (2011) 106–107.
[21] O. Akhavan, E. Ghaderi, ACS Nano 4 (2010) 5731–5736.
[22] W. Hu, C. Peng, M. Lv, X. Li, Y. Zhang, N. Chen, C. Fan, Q. Huang, ACS Nano 5 (2011) 3693–3700.
[23] E. Hashemi, O. Akhavan, M. Shamsara, R. Rahighi, A. Esfandiar, A.R. Tayefeh, RSC Adv. 4 (2014) 27213–27223.
[24] O. Akhavan, E. Ghaderi, A. khavan, Biomaterials 33 (2012) 8017–8025.
[25] O. Akhavan, E. Ghaderi, H. Emamy, F. Akhavan, Carbon 54 (2013) 419–431.
[26] I.Y. Jeon, Y.R. Shin, G.J. Sohn, H.J. Choi, S.Y. Bae, J. Mahmood, S.M. Jung, J.M. Seo, M.J. Kim, D.W. Chang, L. Dai, J.B. Baek, Proc. Natl. Acad. Sci. U. S. A. 109 (2012) 5588–5593.
[27] L. Yan, M. Lin, C. Zeng, Z. Chen, S. Zhang, X. Zhang, A. Wu, Y. Wang, L. Dai, J. Qu, M. Guo, Y. Liu, J. Mater. Chem. 22 (2012) 8367–8371.
[28] L. Yan, Y. Wang, X. Xu, C. Zeng, J. Hou, M. Lin, J. Xu, F. Sun, X. Huang, L. Dai, F. Lu, Y. Liu, Chem. Res. Toxicol. 25 (2012) 1265–1270.
[29] L. Ding, J. Stilwell, T. Zhang, O. Elboudwarei, H. Jiang, J.P. Seleque, P.A. Cooke, J.W. Gray, F.F. Chen, Nano Lett. 5 (2005) 2448–2464.
[30] L. Zhu, D.W. Chang, L. Dai, Y. Hong, Nano Lett. 7 (2007) 3592–3597.
[31] F. Wang, F. Gao, M. Lan, H. Yuan, Y. Huang, J. Liu, Toxicol. in Vitro 23 (2009) 808–815.
[32] L. Feng, Z. Liu, Nanomedicine 6 (2011) 317–324.
[33] X. Zhang, J. Yin, C. Peng, W. Hu, Z. Zhu, W. Li, C. Fan, Q. Huang, Carbon 49 (2011) 986–995.
[34] K. Yang, J.M. Wan, S. Zhang, Y. Zhang, S. Lee, Z. Liu, ACS Nano 5 (2011) 516–522.
[35] L. Yan, G. Li, S. Zhang, F. Sun, X. Huang, Q. Zhang, L. Dai, F. Lu, Y. Liu, Chin. Sci. Bull. 58 (2013) 2347–2353.
[36] R.K. Srivastava, A.B. Pant, M.P. Kashyap, V. Kumar, M. Lohani, L. Jonas, Q. Rahman, Nanotoxicology 5 (2011) 195–207.
[37] J. Bartek, J. Lukas, FEBS Lett. 490 (2001) 117–122.
[38] C.J. Sherr, Cell 116 (2004) 235–246.
[39] N. Lewinski, V. Colvin, R. Drezek, Small 4 (2008) 26–49.
[40] V. Raffa, G. Ciofani, O. Vittorio, C. Riggio, A. Cuschieri, Nanomedicine 5 (2010) 89–97.
[41] T. Fiore, B. Iaccheri, F. Pietrolucci, F. Giansanti, A. Cavaliere, R. Coltella, M.G. Mameli, S. Androudi, P. Brazitikos, C. Cagini, Retina 30 (2010) 1536–1541.
[42] R.P. Manzano, G.A. Peyman, P. Khan, M. Kivilcim, Retina 26 (2006) 257–261.
[43] R.P. Manzano, G.A. Peyman, P.E. Carvounis, M. Kivilcim, P. Khan, P. Chevez-Barrios, Graefes Arch. Clin. Exp. Ophthalmol. 246 (2008) 907–911.